# Model of a Contact Lens and Tear Layer at Static Equilibrium

Bhagya Athukorallage[1] and Ram Iyer[1]

***Abstract*— In this paper, we study the static stability of a spherical cap lens and a tear layer. The contact angle of the tear meniscus with the cornea and contact lens may have a range of values due to capillary effect hysteresis. As the lens is in static equilibrium all the forces and moments sum to zero. Capillary effect hysteresis is found to be a beneficial effect aiding the stability of the lens. The forces acting on the lens are its weight, force due to hydrostatic and atmospheric pressures and surface tension on the periphery of the lens due to the tear meniscus. The fixed parameters in the model are weight of the lens, coefficient of surface tension, magnitude of gravitational acceleration, density of the tear liquid and physical parameters of the lens such as the diameter and base curve radius. The adjustable parameters in the model are contact angles of the tear meniscus with the cornea and contact lens respectively and the position of the lens on the cornea. Numerical experiments suggest that there exists a range of values for the adjustable parameters that lead to physically reasonable solutions, for lens position; extent of overlap of the lower lid on the lens; pressure due to the lid on the lens; and the thickness of tear layer between the lens and the cornea.**

## I. INTRODUCTION

Consider a capillary surface that is in an equilibrium at a vertical flat wall, as depicted in Fig. 1. Assume that the capillary surface is uniform in the $y$ direction. $z(x)$ is the equation of the surface, which asymptotically touches the $X-$axis for all values of $y$, that is, $\lim_{x\to\infty} z(x) = 0$.

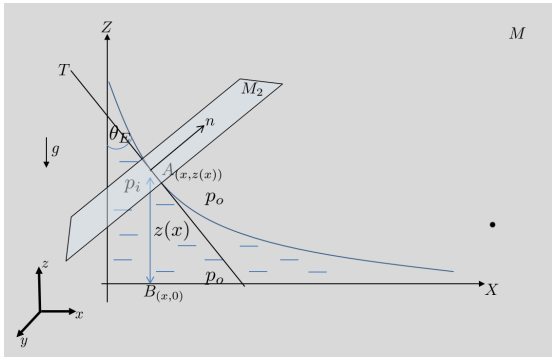


Fig. 1. Capillary surface at a vertical wall. $Z-$axis represents the vertical wall. $M$ and $M_2$ are planes parallel and perpendicular to the $XZ$ plane. $p_o$ is the atmospheric pressure. The dashed region denotes the liquid film at the vertical wall. Contact angle at the vertical wall is $\theta_E$.

The Young-Laplace equation [3] relates the mean curvature of a capillary surface to pressure difference across the surface

$$\delta p = \gamma \left( \frac{1}{R_1} + \frac{1}{R_2} \right). \tag{1}$$

Here, $\delta p$ denotes the pressure difference between the liquid-gas interface, and we define the pressure difference $\delta p$ to be $p_{liquid} - p_{gas}$. $R_1$ and $R_2$ are the principal radii of curvature at a point on the surface. Let the sign of the principal curvature be positive if the center of the corresponding osculating circle [12] lies inside the liquid [9], [23]. In specific situations, we obtain a second-order nonlinear differential equation for the meniscus profile by applying (1).

The same capillary surface given in Fig. 1 possesses potential energy due to surface tension and the pressures due to the presence of a liquid on one side of the surface and atmosphere on the other side. The differential form of the potential energy is [3]

$$d\mathcal{J} = \gamma \, dA - \delta p \, dV. \tag{2}$$

In (2), $\gamma$ is the surface energy per unit area. $dA$ and $dV$ are the surface area and volume elements of the liquid respectively. The potential energy functional is

$$\mathcal{J} = \int d\mathcal{J} = \int_{\partial\Omega} \gamma \, dA - \int_{\Omega} \delta p \, dV, \tag{3}$$

where $\Omega$ is the region occupied by the liquid and $\partial\Omega$ is the boundary of $\Omega$. Both methods result in the same equation for the capillary surface at a vertical wall.

The potential energy functional approach is used to model the tear meniscus around a symmetric, spherical cap lens in Section II-B. We analyze the static equilibrium of the lens by considering all the forces and moments that act on the lens. We consider the following four forces on the lens and ignore the forces due to the upper lid. They are the lens weight, forces due to hydrostatic and atmospheric pressure, surface tension forces on the periphery of the lens due to the tear meniscus and the force due to the lower eyelid. The lens weight acts through its center of mass, parallel to the direction of gravitational acceleration $\mathbf{g}$. Forces result from hydrostatic pressure and atmospheric pressure acting perpendicular to the posterior and anterior sides of the lens respectively. Thus, due to the spherical shape of the contact lens, all these pressure forces and their resultant force have the direction of the outward normal vector to the sphere. Furthermore, surface tension forces act on the lens at the contact line and directed tangentially to the tear meniscus. Since the tear film is at equilibrium, its velocity $\mathbf{u}$ and, hence, viscous stress $\tau$ (refer (5)) are zero. Therefore, in our model, we neglect the force on the posterior side of the lens due to the viscous stress.

[1]B. Athukorallage and R. Iyer are with the Department of Mathematics and Statistics, Texas Tech University, Lubbock, TX 79409 USA. bhagya.athukorala at ttu.edu and ram.iyer at ttu.edu

We use the lens weight, coefficient of surface tension, density of the tear liquid, magnitude of gravitational acceleration, lens diameter and its base curve radius as the fixed parameters. The adjustable parameters in our model are the position of the lens on the cornea, contact angle of the tear meniscus with the cornea and contact lens respectively. Due to the contact angle hysteresis phenomenon, which is discussed in more detail in section II-A, the contact angles may take values in a closed interval instead of taking a single value.

Our mathematical model for the tear meniscus is valid for rigid gas permeable (RGP) lenses as well as for the soft contact lenses. However, numerical simulations are done only for the RGP type lenses. Our numerical calculations show that the pressure change due to gravity significantly affect the equilibrium equations. In particular, the force resultant due to hydrostatic pressure is greater than the surface tension force in the $z$ direction.

In addition to ignoring the change in hydrostatic pressure due to gravity, the capillary effect is also ignored in [1] and in [18]. These forces are significant and cannot be ignored as shown in this paper. The net force due to hydrostatic pressure has the largest magnitude amongst all the forces acting on a lens and the capillary effect reduces the magnitude of the lid (or other) forces needed to maintain static equilibrium.

In the literature [1], the contact lens and tear meniscus are considered to be in a quasi-static equilibrium state. The author assumes the shape of the contact lens to be a cylindrical shell type with a unit width. Reaction force due to the posterior tear film, upper and lower contact angles are calculated by considering the quasi-static equilibrium of the lens in two-dimensions. However, calculation of the reaction force due to the posterior tear film completely neglects hydrostatic pressure variation due to gravity. But, our numerical simulations show that the force due to hydrostatic pressure significantly affects the static equilibrium of the lens. The literature [2] models the contact lens and the cornea as flat surfaces with infinite width. Lubrication approximation theory is used to model quasi-steady motion of the tear film under the contact lens and away from the lens. In the analysis of the the latter tear film, its attachment to the cornea is incorrectly modeled. As a result, gravitational force acting on the fluid is neglected in the analysis. In [18], the contact lens considered is a porous, planar, circular disk, and the authors model the dynamics of the contact lens during blinking. They use a version of Darcy's law to model constitutive relation of tear, in which gravity is neglected. For the no blink or quasi-static blink case, this constitutive relation yields a constant pressure distribution in the tear layer, which is unphysical.

In our analysis, we consider the static equilibrium of a spherical lens in three-dimensions by introducing an additional force that results from the lower eyelid. Effect of hydrostatic pressure includes in the equilibrium equations of the lens. We assume linear variations of the contact angles of the tear meniscus with the lens. Ranges of values for the adjustable parameters are obtained through the numerical simulations for the static equilibrium of the lens.

## II. TEAR MENISCUS AROUND A CONTACT LENS

### A. Contact angle hysteresis

Consider a liquid droplet on a solid surface with a contact angle of $\theta$ (refer to Fig. 2). Experiments show that if the liquid is carefully added to the droplet via a syringe, the volume and contact angle of the droplet will increase without changing its initial contact area. Further increase of its volume results in an increase in the contact area with the contact angle fixed at $\theta_A$ (refer to Fig. 2(a)). Similarly, if the liquid is removed from a droplet, volume and contact angle of the droplet decrease, but retain the same contact area. Continuing this process results in a recession of the contact area at a contact angle of $\theta_R$ (refer to Fig. 2(b)) [3], [5]. These two limiting values, $\theta_A$ and $\theta_R$, are referred to as *advancing* and *receding angles*.

Fig. 3 indicates the hysteresis loops (ABCDA and ABEFA) that are numerically obtained by calculating the pressure difference ($\delta p$) of the inside and outside of a liquid droplet with its volume. Point A corresponds to the starting point of the both cycles. Let the contact angle of the droplet be $\theta_i$. Increasing of the droplet volume results in the increasing of the contact angle $\theta_i$, and the corresponding variation of $\delta p$ with the droplet volume is depicted in the path A-B. Once the value of $\theta_i$ reaches to $\theta_A$, contact line of the droplet moves to a new stable position (B-C). Next, liquid is removed from the newly formed droplet and this results in a decreasing of the contact angle, and continuing this process yields $\theta_i$ to reach $\theta_R$ (C-D). Finally, at the value of $\theta_R$, contact line of the droplet moves to its initial position (D-A). Loop ABEFA is obtained through a similar method as the loop ABCDA, reducing the volume of the droplet after $\theta_i$ reaches to the value of $\theta_A$ and before contact line reaches to a new stable position. Note that the curves A-B, C-D and E-F are reversible paths. Consider the hysteresis loop ABCDA. The integrals on paths AB and BC represent the work that must be done by the droplet (the external agency, which is increasing the volume) against the surrounding. The integrals on paths CD and DA represent the work done by the surrounding on the droplet. Thus, the area of the hysteresis loop ABCDA is the net work that must be done by the droplet (or the external agent) against the surrounding.

### B. Modeling the tear meniscus around a contact lens

In this endeavor, the tear meniscus is considered that forms between the cornea and a contact lens. In the Cartesian coordinate system shown in Fig. 4, the domains bounded by the

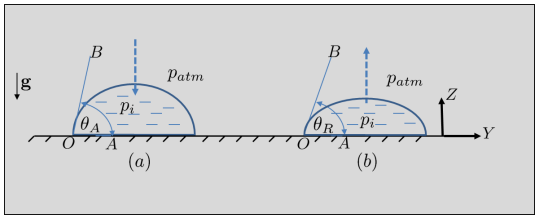


Fig. 2. Advancing and receding contact angles of a liquid drop.

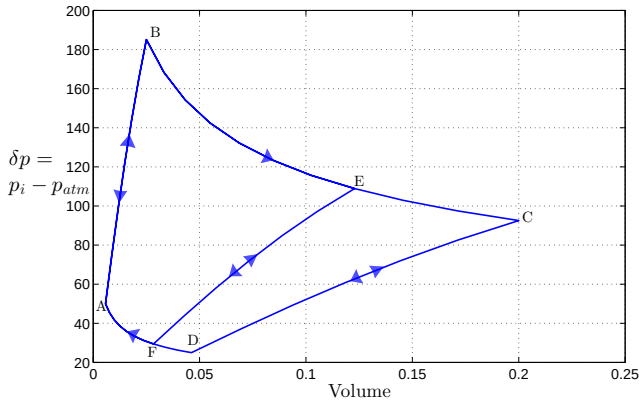


Fig. 3. Hysteresis curves for a liquid drop. $\delta p$ indicates the pressure difference between the liquid-gas interface of a liquid drop. Points B and C correspond to the advancing and receding contact angles of the droplet.

contact lens and tear meniscus are $\Omega_1$ and $\Omega_2$ respectively. Furthermore, the contact line formed between the lens and the meniscus is denoted by $\partial\Omega_{12}$. Inner and outer profiles of a contact lens have the equations $F_i(x,y)$ and $F_o(x,y)$ respectively. Moreover, we introduce a rotational motion of the contact lens around the $y$ axis by adding a linear function, $z(x) = m\,x + b$. Let the pressure developed inside the tear meniscus be $p_i(x,y,z)$ and the profile of the tear meniscus be $z = f(x,y)$. Finally, atmospheric (outer) pressure, $p_{atm}$ is assumed to be a constant throughout the domains.

Consider the potential function that is defined by (2). Surface energy per unit area is taken to be a constant in a given domain. Then the total energy of the system is given by

$$\begin{aligned}\mathcal{J} &= \int_{\Omega_2}\gamma\,dA - \int_{\Omega_2}\delta p_2(x,y,z)\,dV_t \\ &\quad - \int_{\Omega_1}\delta p_1(x,y,z)\,dV_t - \int_{\Omega_1}\rho_c\,g\,x\,dV_l, \end{aligned} \tag{4}$$

where subscripts $t$ and $l$ refer to the quantities involving tear and lens. $\rho_c$ is the density of the lens and $g$ is the magnitude

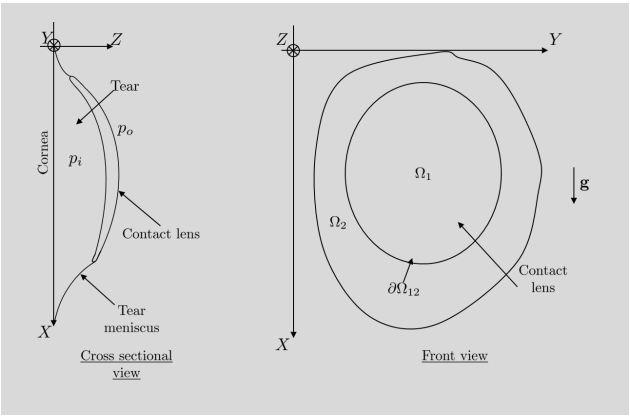


Fig. 4. Contact lens on a cornea. $\mathbf{g}$ acts along the $X$ direction. Tear pressure and atmospheric pressure are $p_i$ and $p_{atm}$ respectively. Domain of the lens is $\Omega_1$ and the domain of the tear meniscus is $\Omega_2$.

of gravitational acceleration. The term $\int_{\Omega_1}\rho_c\,g\,x\,dV_l$ in (4) is the potential energy of the contact lens.

Consider the Cauchy momentum equation [7]:

$$\rho\frac{D\mathbf{u}}{Dt} = \rho\mathbf{g} - \nabla p + \nabla\cdot\tau, \tag{5}$$

where $\tau = \mu\left(\dfrac{\nabla\mathbf{u} + \nabla\mathbf{u}^T}{2}\right)$.

In (5) $\rho$ and $\mu$ denote the density and the viscosity of the fluid. Furthermore, $\mathbf{u}$ and $\tau$ are the velocity of the fluid and its viscous stress. $\mathbf{g}$ is the vector $(g,0,0)^T$ where $g$ represents the magnitude of the gravitational acceleration. $\nabla$ is the gradiant operator in three-dimensions and $\frac{D}{Dt}$ is the operator $\frac{\partial}{\partial t} + \mathbf{u}\cdot\nabla$ .

For a static Newtonian fluid, (5) can be simplified to

$$\nabla p(x,y,z) = \rho\mathbf{g}. \tag{6}$$

Solutions of (6) for $p(x,y,z)$ yields a function $p(x)$ that is dependent on $x$ alone:

$$p(x) = \rho g x + p_i(0), \tag{7}$$

where $g$ is the gravitational constant and $p_i(0) = p|_{x=0}$. Thus, pressure difference between the liquid-gas interface is

$$\begin{aligned}\delta p &= p(x) - p_{atm}, \\ &= \rho_t g x + p_i(0) - p_{atm}. \end{aligned} \tag{8}$$

According to the given configuration of the coordinate system, any point on the capillary surface can be described by the parameterization,

$$\mathbf{r}(x,y) = (x,y,f(x,y)). \tag{9}$$

Then, surface area, $A$ of a given domain $\Omega$ is

$$\begin{aligned}A &= \iint_{\Omega}\left|\frac{\partial\mathbf{r}}{\partial x}\times\frac{\partial\mathbf{r}}{\partial y}\right|dx\,dy, \\ &= \iint_{\Omega}\sqrt{1+f_x^2+f_y^2}\,dx\,dy. \end{aligned} \tag{10}$$

Substitute (8) and (10) into (4) leads to

$$\begin{aligned}\mathcal{J}(f,m) &= \iint_{\Omega_2}\gamma\sqrt{1+f_x^2+f_y^2} - (\rho_t g x + p_i(0) - p_{atm})f\;dxdy \\ &- \iint_{\Omega_1}(\rho_t g x + p_i(0) - p_{atm})(F_i + mx + b)\;dxdy \\ &- \iint_{\Omega_1}\rho_c g x[F_o(x,y) - F_i(x,y)]\;dxdy, \end{aligned} \tag{11}$$

subject to the constraint

$$f(x,y) = F_i(x,y) + mx + b \qquad \forall\,(x,y)\in\partial\Omega_{12}. \tag{12}$$

Thus, the modified functional:

$$\bar{\mathcal{J}}(f,m,b,\lambda) = \mathcal{J}(f,m) + \lambda(F_i + mx + b - f) \tag{13}$$

where $\lambda$ represents the Lagrange multiplier.
Equation (13) has the form

$$\bar{\mathcal{J}}(f,m,b,\lambda) = \iint_{\Omega_1} \mathcal{L}_1(x,y,m,b)\,dxdy + \iint_{\Omega_2} \mathcal{L}_2(x,y,f,f_x,f_y)\,dxdy. \quad (14)$$

For simplicity of analysis, we consider $m$ and $b$ to be fixed. These are the cases we consider in the rest of the paper.
Thus, associated Euler - Lagrange equation of (14) on $\Omega_2$ is,

$$\frac{\partial \mathcal{L}_2}{\partial f} - \frac{\partial}{\partial x}\frac{\partial \mathcal{L}_2}{\partial f_x} - \frac{\partial}{\partial y}\frac{\partial \mathcal{L}_2}{\partial f_y} = 0, \quad (15)$$

Simplifying (15) we get,

$$\frac{p_{atm}-p_i(0)-\rho_t g x}{\gamma} = \frac{(1+{f_y}^2)f_{xx} + (1+{f_x}^2)f_{yy} - 2f_x f_y f_{xy}}{(1+{f_x}^2+{f_y}^2)^{\frac{3}{2}}}. \quad (16)$$

### C. Two-dimensional analysis of tear meniscus

We begin our study by considering the idealized case of a flat and rectangular contact lens of unit width, and a flat corneal wall (refer to Fig. 5). Consider (16) that is derived in the previous section for the meniscus profile. The meniscus profile depends on the $x$ variable only.

Then from (16), the equation for the upper meniscus profile is,

$$\frac{p_{atm} - p_i(0) - \rho_t g x}{\gamma} = \frac{f_{xx}}{(1+{f_x}^2)^{\frac{3}{2}}}, \quad (17)$$

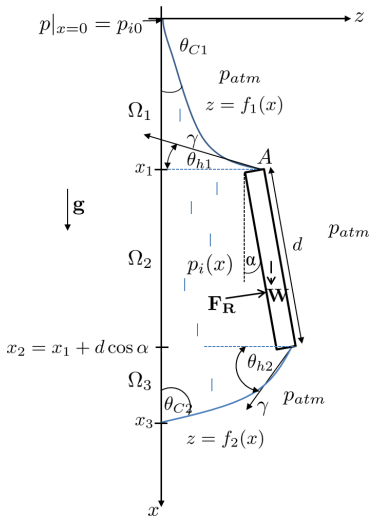


Fig. 5. The upper and lower tear menisci on a section of a contact lens for the idealized case when the cornea and the contact lens are flat, and the contact lens is rectangular. The angle of tilt of the lens is $\alpha$. $\theta_{C1}$ and $\theta_{C2}$ denote the contact angle on the upper and lower cornea respectively. $\theta_{L1}$ and $\theta_{L2}$ represent the upper and the lower contact angle between the tear meniscus and the contact lens. $\mathbf{F_R}$ is the resultant force due to the fluid pressure on the posterior and anterior sides of the lens.

with the boundary conditions, $f(0) = 0$ and $f_x(0) = \tan\theta_{C1}$.
Convert (17) in to a first order system of ODE results,

$$y_1' = y_2, \quad (18)$$

$$y_2' = (1+y_2^2)^{3/2}\left(\frac{p_{atm} - p_i(0) - \rho g x}{\gamma}\right). \quad (19)$$

Moreover, (19) has the form

$$y_2' = (1+y_2^2)^{3/2}(k - cx) \quad (20)$$

where $k = \frac{p_{atm} - p_i(0)}{\gamma}$ and $c = \frac{\rho g}{\gamma}$. Equation (20) may be integrated to find the solution

$$\sin(\tan^{-1} y_2) = kx - \frac{cx^2}{2} + C_0. \quad (21)$$

The value of $C_0$ in (21) is determined using the boundary condition, $y_2(0) = f_x(0) = \tan\theta_{C1}$.
Thus,

$$y_2(x) = \tan\left(\sin^{-1}\left(kx - \frac{cx^2}{2} + \sin\theta_{C1}\right)\right). \quad (22)$$

As $y_2(x) = f_x = \tan\beta$, where $\beta$ is the angle depicted in Fig. 6 and its value is given by

$$\beta = \tan^{-1} y_2 = \sin^{-1}\left(kx - \frac{cx^2}{2} + \sin\theta_{C1}\right). \quad (23)$$

Since $\beta \in [0, \frac{\pi}{2}]$, (23) implies

$$0 \le kx - \frac{cx^2}{2} + \sin\theta_{C1} \le 1$$
$$\Rightarrow \quad 0 \le cx^2 - 2kx + 2(1-\sin\theta_{C1}) \le 2. \quad (24)$$

Consider the compound inequality in (24).

- $cx^2 - 2kx + 2(1-\sin\theta_{C1}) \ge 0 \ \ \forall \ \ x \ge 0$

$$\Rightarrow k \le \sqrt{\frac{2\rho g(1-\sin\theta_{C1})}{\gamma}}$$

$$\Rightarrow p_i(0) \ge p_{atm} - \sqrt{2\rho g\gamma(1-\sin\theta_{C1})} \qquad \forall\, x \ge 0. \quad (25)$$

- $2 \ge cx^2 - 2kx + 2(1-\sin\theta_{C1})$

$$0 \ge cx^2 - 2kx - 2\sin\theta_{C1} = g(x) \quad (26)$$

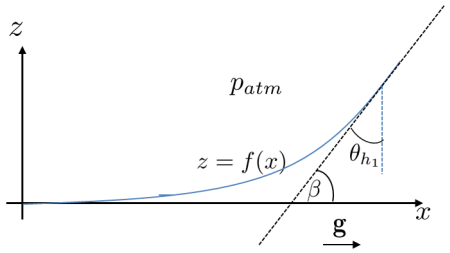


Fig. 6. Upper tear meniscus profile, $z = f(x)$, on the rectangular contact lens when the cornea and the contact lens are flat. Gravity $\mathbf{g}$ acts in the $x$ direction. $\theta_{h1}$ is the angle between the tear meniscus and an axis parallel to the $z$ axis, and $\theta_{h1} = \frac{\pi}{2} - \beta$.

Since $c > 0$, graph of $g(x)$ is convex. Thus, in order to satisfy (26), $x \in [x_1, x_2]$, where

$$x_1 = \frac{k - \sqrt{k^2 + 2\sin\theta_{C1}}}{c} \quad \text{and} \quad x_2 = \frac{k + \sqrt{k^2 + 2\sin\theta_{C1}}}{c}. \tag{27}$$

Since $x_1 < 0$ and $x_2 > 0$, if $x \in [0, x_2]$, the inequalities in (24) are satisfied.

For static equilibrium, the net force and net moment on the lens must be zero. Numerical computations [23] show that the net force due to the pressure difference between the anterior and posterior sides of the lens is significantly larger in magnitude than that due to the surface tension (see Fig. 7). Furthermore, we see that a force in addition to the ones displayed in Fig. 5 - namely, the weight, surface tension, and pressure difference - is needed to stabilize the lens. This additional force could presumably be due to either the upper or lower lid. These conclusions are useful in the next section on the modeling of the spherical cap lens.

### *D. Three-dimensional analysis of a tear meniscus with a spherical cap type contact lens*

In this section, we consider a lens that has a shape of a spherical cap. For simplicity, tilting angle, $\alpha$ of the cap is assumed to be zero. The lens and the upper tear meniscus are modeled with a lower eyelid force, $\mathbf{F_L}$.

The radius and a uniform thickness of the spherical cap are assumed to have the values of $R$ and $t$ respectively. The center of the cap is denoted by $O$ and the origin of the spherical coordinate system is placed at that point $O$ as shown in Fig. 8. The apex angle of the cap is symbolized by $2\bar{\theta}$.

In the following analysis, the centroid of the cap is located based on its moment about the $xy$, $xz$ and $yz$ planes. However, since the cap is symmetric about the $x$ and $y$ axis, the centroid has the coordinates of the form $(0, 0, z_c)$, where $z_c$ denotes the $z$ coordinate of the centroid. As shown in

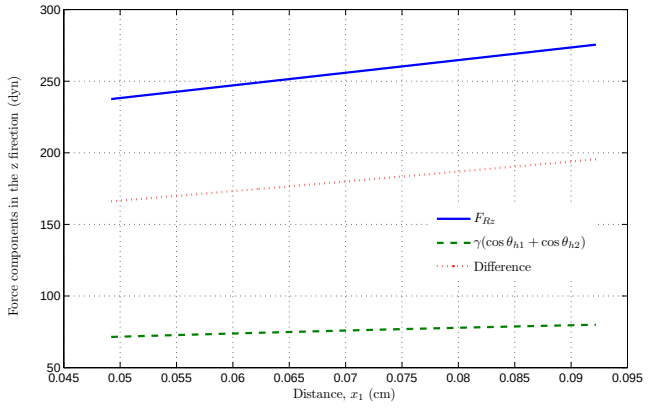


Fig. 7. Force components in the $z$ direction. $\mathbf{F_{Rz}}$ is the resultant force component in the $z$ direction due to the liquid pressure on the lens. $\gamma(\cos\theta_{h1} + \cos\theta_{h2})$ denotes the only force component in the $-z$ direction. This force component results from the surface tension forces on the lens. The difference between the above mentioned components is positive for all feasible $x_1$ values.

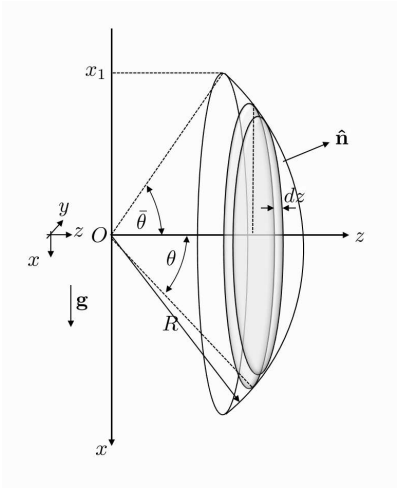


Fig. 8. Spherical cap type contact lens. The radius and apex angle of the spherical cap are $R$ and $2\bar{\theta}$ respectively. $\hat{\mathbf{n}}$ is the unit normal in the radial direction. $\mathbf{g}$ acts in the $x$ direction. The width and apex angle of the spherical frustum are $dz$ and $2\theta$.

Fig. 8, we consider a spherical frustum on the cap that has an angle $\theta$ from the $z-$axis with a width of $dz$. Let the material density of the lens be $\rho$. Thus, the moment about $xy$ plane results

$$z_c = \frac{1}{W}\int_0^{\bar{\theta}} 2\pi R^3 \rho t \sin^2\theta\cos\theta\, d\theta \tag{28}$$

$$\text{where} \quad W = \int_0^{\bar{\theta}} 2\pi R^2 \rho t \sin^2\theta\, d\theta. \tag{29}$$

By using (28) and (29), the $z$ coordinate of the centroid turns to be

$$z_c = \frac{2R\sin^3\bar{\theta}}{3\left(\bar{\theta} - \dfrac{\sin 2\bar{\theta}}{2}\right)}. \tag{30}$$

Let the unit vector in the radial direction be $\hat{\mathbf{n}}$ and it is denoted by

$$\hat{\mathbf{n}} = (\sin\theta\cos\phi, \sin\theta\sin\phi, \cos\theta). \tag{31}$$

Next, we consider the forces that act on the lens. Since our lens has a spherical profile, forces due to hydrostatic pressure act radially in the outward direction, that is, in the direction of $\hat{\mathbf{n}}$. Therefore, the liquid force $\mathbf{dF_R}$ on an area element, $R^2\sin\theta\, d\theta\, d\phi$ on the spherical cap (refer to Fig. 9) is given by

$$\mathbf{dF_R} = (p_i(x) - p_{atm})R^2\sin\theta\, d\theta\, d\phi\, \hat{\mathbf{n}} \tag{32}$$

where

$$p_i(x) = p_i(0) + \rho g x_1 + \rho g R\sin\bar{\theta} + \rho g R\sin\theta\,\cos\phi. \tag{33}$$

Thus, the total resultant force due to the liquid pressure $\mathbf{F}_R$, on the spherical cap is found using (32) and (33).

$$\mathbf{F}_R = \int_0^{\bar{\theta}}\int_0^{2\pi} (p_i(x) - p_{atm})R^2\sin\theta\,\hat{\mathbf{n}}\, d\theta\, d\phi. \tag{34}$$

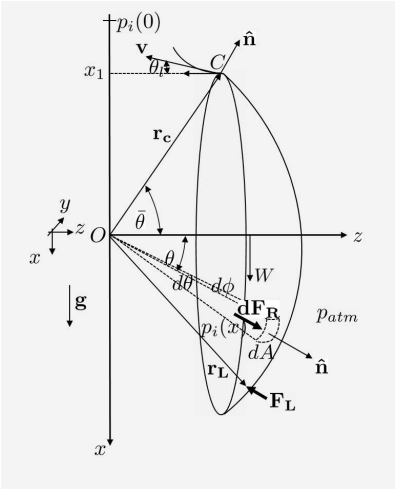


Fig. 9. Forces acting on the spherical cap. $\mathbf{F_L}$ and $\mathbf{r_L}$ denote the lower eyelid force and its position vector with respect to the coordinate system. Gravity $\mathbf{g}$ acts in the $x$ direction. Contact angle $\theta_l$ is the angle between the tear meniscus and the lens at distance $x_1$. $\mathbf{dF_R}$ is the force acting on an area element $dA$ due to the liquid pressure.

Hence, its components in the $x$, $y$ and $z$ directions are

$$\begin{aligned} F_{Rx} &= \rho g \pi R^3 \left( \frac{2}{3} - \cos\bar{\theta} + \frac{\cos^3\bar{\theta}}{3} \right), \\ F_{Ry} &= 0, \\ F_{Rz} &= \frac{c_1 \pi R^2}{2} (1 - \cos 2\bar{\theta}) \end{aligned} \tag{35}$$

respectively and $c_1 = p_i(0) + \rho g x_1 + \rho g R \sin\bar{\theta} - p_{atm}$.

Surface tension forces act along the circumference of the spherical cap in the direction of the tear meniscus. Let $\mathbf{v}$ be a vector pointing tangent to the tear meniscus from a point, $C$, on the circumference of the spherical cap. An orthonormal basis for the plane described by the span of $-\hat{\mathbf{k}}$ and $\hat{\mathbf{n}}$ is

$$\left\{ -\hat{\mathbf{k}}, \frac{\hat{\mathbf{n}} - \hat{\mathbf{k}}(\hat{\mathbf{k}} \cdot \hat{\mathbf{n}})}{||\hat{\mathbf{n}} - \hat{\mathbf{k}}(\hat{\mathbf{k}} \cdot \hat{\mathbf{n}})||} \right\}. \tag{36}$$

The vector $\mathbf{v}$ in this orthonormal basis is given by

$$\mathbf{v} = -\cos\theta_l \hat{\mathbf{k}} + \sin\theta_l \left( \frac{\hat{\mathbf{n}} - \hat{\mathbf{k}}(\hat{\mathbf{k}} \cdot \hat{\mathbf{n}})}{||\hat{\mathbf{n}} - \hat{\mathbf{k}}(\hat{\mathbf{k}} \cdot \hat{\mathbf{n}})||} \right). \tag{37}$$

As $\hat{\mathbf{n}} = (\sin\theta\cos\phi, \sin\theta\sin\phi, \cos\theta)^T = \sin\theta\cos\phi\,\hat{\mathbf{i}} + \sin\theta\sin\phi\,\hat{\mathbf{j}} + \cos\theta\,\hat{\mathbf{k}}$, the coordinates for the vector $\mathbf{v}$ are:

$$\mathbf{v} = (\sin\theta_l\cos\phi, \sin\theta_l\sin\phi, -\cos\theta_l) \tag{38}$$

where $\theta_l$ denotes the contact angle at the point $C$ (refer to Fig. 9). Let the diameter of the lens be $D$.

Then the total force due to surface tension $(\mathbf{S})$ is given by the following equation,

$$\mathbf{S} = \int_0^{2\pi} \frac{\gamma D}{2}\, \mathbf{v}\, d\phi \tag{39}$$

Then, force equilibrium of the lens yields,

$$\mathbf{F}_R + \mathbf{W} + \mathbf{S} + \mathbf{F}_L = 0. \tag{40}$$

Finally, we consider the moment of the forces, $\mathbf{F}_R$, $\mathbf{F}_L$, $\mathbf{S}$ and $\mathbf{W}$ about the point $O$. Since the resultant force, $\mathbf{F}_R$ acts normal to the spherical cap, its moment about the point $O$ is zero.

Let the position vector of the centroid be denoted by $\mathbf{r}_W$. Thus, the moment due to the weight $(\mathbf{M}_W)$ is defined by the equation,

$$\mathbf{M}_W = \mathbf{r}_W \times \mathbf{W} = \begin{pmatrix} 0 \\ \dfrac{2RW\sin^3\bar{\theta}}{3\left(\bar{\theta} - \dfrac{\sin 2\bar{\theta}}{2}\right)} \\ 0 \end{pmatrix}. \tag{41}$$

Next, the moment resulted due to the surface tension is considered about the point $O$. We denote the vector, $\mathbf{r}_c$ of a point $C$, on the base circle of the spherical cap by,

$$\mathbf{r}_c = (R\sin\bar{\theta}\cos\phi, R\sin\bar{\theta}\sin\phi, R\cos\bar{\theta}). \tag{42}$$

Hence, using (38) and (42), the moment of the surface tension at the point $C$ is expressed as $\mathbf{M}_{S_c} = \mathbf{r}_c \times \gamma\mathbf{v}$ and then, the total momentum of surface tension yields to be

$$\begin{aligned} \mathbf{M}_S &= \int_0^{2\pi} \frac{\gamma D}{2} (\mathbf{r} \times \mathbf{v})\, d\phi \\ &= \frac{RD\gamma}{2} \int_0^{2\pi} \sin(\bar{\theta} + \theta_l) \begin{pmatrix} -\sin\phi \\ \cos\phi \\ 0 \end{pmatrix} d\phi. \end{aligned} \tag{43}$$

Now, assume the lid force $\mathbf{F}_L$ has the components $F_{Lx}$, $F_{Ly}$ and $F_{Lz}$ in the directions of $x$, $y$ and $z$ respectively. Let $\mathbf{r}_L$ be a vector corresponding to the point $L$, where the force $\mathbf{F}_L$ acts on the surface of the spherical cap. Hence, the moment of $\mathbf{F}_L$ about the point $O$ is,

$$\begin{aligned} \mathbf{M}_L &= \mathbf{r}_L \times \mathbf{F}_L \\ &= R \begin{pmatrix} F_{Lz}\sin\theta\sin\phi - F_{Ly}\cos\theta \\ F_{Lx}\cos\theta - F_{Lz}\sin\theta\cos\phi \\ F_{Ly}\sin\theta\cos\phi - F_{Lx}\sin\theta\sin\phi \end{pmatrix} \end{aligned} \tag{44}$$

Furthermore, using the facts that $F_{Ry} = 0$ and $S_y = 0$, we conclude that $F_{Ly} = 0$. Thus, applying the aforementioned facts with the help of (44), we obtain the following two results at the point $L$.

$$\phi = 0, \qquad \theta = \tan^{-1}\left(\frac{F_{Lx}}{F_{Ly}}\right). \tag{45}$$

Finally, for the equilibrium of the lens,

$$\mathbf{M}_W + \mathbf{M}_S + \mathbf{M}_L = 0. \tag{46}$$

We numerically calculate all the forces and the moments in the $x$, $y$ and $z$ direction for all the possible contact angles at the point $(R, \pi, \bar{\theta})$. Possible overlap distances $L$ for the lower eyelid are numerically calculated by considering the equilibrium of the lens. In the literature [22], the values of the contact angle for the tear meniscus with the contact lens $(\theta_l)$ are reported to be in the interval $[10°, 50°]$. Thus, we let $\theta_l = \theta_l(\phi)$, where the angle $\phi$ represents the azimuthal angle of the spherical coordinate system. Our hypothesis is also

verified by the contact angle hysteresis phenomenon which is in Section II-A.

For the numerical calculation, we consider a linear variation of $\theta_l$ with respect to the angle $\phi$. Maximum value of the contact angle, which occurs at $(R, \pi, \bar{\theta})$, is computed from $(23)$ according to as explained in Fig. 6. This is an approximation as it neglects the curvature in the $\phi$ direction. The minimum value of the contact angle, which occurs at $(R, 0, \bar{\theta})$ is set at $10^\circ$ [22]. Equations (39) and (43) are numerically integrated using the *Simpson's 1/3rd rule*. Parameter values that are used in this calculation are given in Table I.

Fig. 10 shows the variation of forces that act on the lens with respect to the $x_1$ values for the corneal contact angle of $35^\circ$. As depicted in Fig. $10(a), (b)$ and $(c)$, the eyelid force $\mathbf{F_L}$ is necessary for the equilibrium of the lens. Note that hydrostatic force component in the $y$ direction is zero as derived in (35). Variation of the lid overlap distance $L$ is shown in Fig. 10(d).

### *E. Comparison with observations*

In the literature [8], the value of the corneal cap radius is reported to be in the interval $[7.2mm, 8.7mm]$. In our analysis so far, we had assumed a flat and vertical cornea. The numerical results reported in Section II-D were obtained with this assumption. Furthermore, the analysis of Section II-D shows that there are no feasible solutions when the corneal contact angle is less than $32^\circ$.

In this section, we show that there is a satisfactory explanation by considering a curved corneal wall that is inclined at an angle with respect to the vertical at the point of attachment of the tear meniscus. In Fig. 11, the origin is this point of attachment of the meniscus with the curved cornea. We denote the contact angles of the tear meniscus with the flat vertical wall and curved corneal surface by $\theta_{EM}$ and $\theta_{Em}$ respectively (refer to Fig. 11). We numerically calculate the three relevant factors: $(i)$ distance from the origin to the point of attachment of the tear meniscus with the lens $(x_1)$, $(ii)$ average tear film thickness (ATFT), and $(iii)$ radius of the cornea (R) by considering both the flat, vertical cornea, and curved cornea. Numerical calculations show that there are physically reasonable solutions for the aforementioned factors for some $\theta_{EM}$ and $\theta_{Em}$.

We numerically obtain the radius of the cornea $(R)$ and the tear film thickness $(t_i)$ at some point, $x_i$ on the $x-$axis (refer to Fig. 11) using the equations

$$\begin{aligned} R &= \frac{x_1 + D/2}{\sin\alpha} \quad \text{and} \\ t_i &= B_R \cos\tilde{\beta} - R\cos\tilde{\alpha} - (O_1P - O_2P). \end{aligned} \tag{47}$$

In (47), $O_1P = R\cos\alpha + z_1$ and $O_2P = B_R\cos\beta$.

As depicted in the Table II, it is possible to obtain the physically reasonable solutions for the average tear film thickness and radius of the cornea for some contact angles of the tear meniscus with the flat vertical wall and curved corneal surface.

In the preceding section, we defined $\theta_l$ to be a function of the azimuthal angle $\phi$. Next, we extend our analysis to study the static equilibrium of the lens that has a constant contact angle , $\theta_l(\phi) = \theta_0$ along the circumference of the lens. For $\theta_0 = 35^\circ, 40^\circ, 50^\circ$, we numerically compute the parameters, $L$, $\mathbf{F_L}$, ATFT, $R$ and the pressure due to the lower eyelid $(p)$. Similarly, the same parameters are obtained for contact angle $\theta_l(\phi)$ that lies in the interval $[10^\circ, \theta_0]$. These results show that eyelid pressure obtained from the former case yields a greater value than that of the latter case for each $\theta_0$ (refer Table III). For $\theta_l(\phi) = 50^\circ$, ranges of $x_1$ and the angle between the upper tear meniscus and an axis parallel to the $z-$axis $\theta_{h1}$ (refer Fig. 6) become $[0, 2.14]mm$ and $[34.5^\circ, 44.5^\circ]$. Hence, at this particular contact angle there are no feasible solutions for the parameters. As far as the static equilibrium is concerned, the above analysis indicates the latter case yields better results than the former case.

TABLE I

FIXED PARAMETER VALUES FOR THE CASE WHEN THE CORNEA IS FLAT AND THE CONTACT LENS HAS A SPHERICAL CAP SHAPE. THE VALUES OF $\{\rho, g\}$, $\{\theta_c\}$ AND $\{\theta_{min}, \theta_{max}\}$ MAY BE FOUND [1] AND [22] RESPECTIVELY.

| Parameter | Value | CGS units | Parameter | Value | CGS units |
|---|---|---|---|---|---|
| $\rho$ | 1 | $g/cm^3$ | $D$ | 0.98 | $cm$ |
| $g$ | 981 | $cm/s^2$ | $W$ | $0.0152g$ | $dyn$ |
| $\gamma$ | 68 | $dyn\ cm$ | $p_{atm}$ | $10^6$ | $dyn/cm^2$ |
| $R$ | 0.65 | $cm$ | $[\theta_{min}, \theta_{max}]$ | $[10, 50]$ | $deg$ |
| $\theta_c$ | $[30, 50]$ | $deg$ | | | |

## III. CONCLUSIONS

In this research, we mathematically modeled a tear meniscus around a symmetric, spherical cap lens that was at static equilibrium, using a calculus of variations approach.

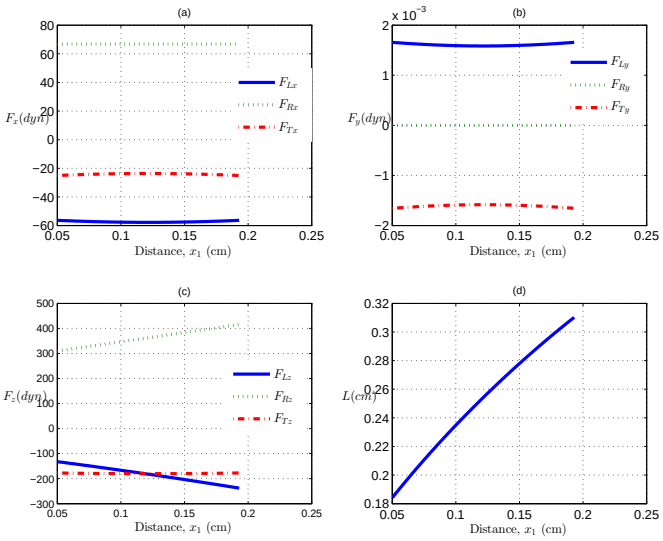


Fig. 10. Variation of the force due to fluid pressure $\mathbf{F_R}$, surface tension $\mathbf{F_T}$ and the lid force $\mathbf{F_L}$ in the $x$, $y$ and $z$ directions. Bottom right corner figure indicates the lid overlap distance $L$.

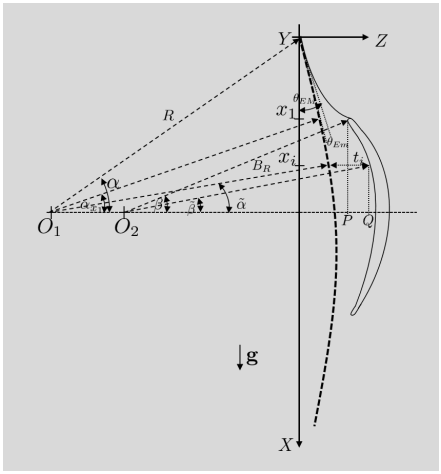


Fig. 11. Contact angles between the tear meniscus with the flat vertical wall and corneal surface. $\theta_{EM}$ and $\theta_{Em}$ denote the contact angles between the tear meniscus with the flat vertical wall and corneal surface respectively. $x_1$ is the upper tear meniscus height. $z_1$ denotes the tear meniscus height from the vertical wall at $x_1$.

Static equilibrium was analyzed by taking the net force and net moment to be zero. The results discussed below assume a flat cornea. We obtained a range of values for the adjustable parameters, the corneal contact angle $\theta_E$, upper contact angle $\theta_{L1}$ and lens position $x_1$ through numerical simulations. There were no solutions for $\theta_E$ in the range $[0°, 31°]$. For $\theta_E = 35°$, our numerical analysis showed that the static equilibrium may be achieved for $x_1$ in the interval $[0.050, 0.193]cm$. The analysis further showed that the pressure force dominated surface tension and the weight of the lens. Hence, for the equilibrium of the lens, it was necessary to introduce the lower lid force $\mathbf{F_L}$. When we increased the value of $\theta_E$ from 35° to 50°, ranges of $x_1$ and the lid overlap distance $L$ became $[0, 2.14]\,mm$ and $[1.05, 3.23]\,mm$ respectively. At this particular corneal contact angle, the magnitude of the lower eyelid force $\mathbf{F_L}$ was between $[143.5, 245.0]\,dyn$. The pressure due to the lower lid when the lid overlap was between $1.84\,mm - 3.10\,mm$ was in the range $0.92\,mm\,Hg - 1.12\,mm\,Hg$, with lesser value for lid overlap corresponding to higher lid pressure. This compares well with the intraocular pressure of $10\,mm\,Hg - 20\,mm\,Hg$ [21]. We numerically calculated the average tear film thickness (ATFT) for a curved cornea, and the moderate values for the ATFT were between $93\,\mu m - 185\,\mu m$ [10]. Therefore, we showed that there exists physically reasonable solutions for a contact lens in static equilibrium for the adjustable parameter values.

TABLE II

REASONABLE SOLUTIONS FOR THE CORNEAL RADIUS AND AVERAGE TEAR FILM THICKNESS AND CORRESPONDING CONTACT ANGLES $\theta_{EM}$ AND $\theta_{Em}$.

| $[\theta_{EM}, \theta_{Em}]$ $(deg)$ | R $(mm)$ | ATFT $(\mu m)$ | $x_1(\mu m)$ |
|---|---|---|---|
| $[40, 5]$ | 8.54 | 133 | 1 |
| $[41, 5]$ | 8.34 | 104 | 1 |
| $[42, 5]$ | 8.14 | 93 | 1 |
| $[43, 5]$ | 7.96 | 99 | 2 |
| $[44, 10]$ | 8.76 | 185 | 1 |
| $[45, 10]$ | 8.54 | 155 | 1 |

TABLE III

PARAMETER VALUES FOR $\theta_0 = 35°, 40°$ AND $50°$.

| $\theta_l\,(deg)$ | $L\,(mm)$ | $\mathbf{F_L}\,(dyn)$ | ATFT $(\mu m)$ | $R\,(mm)$ | $p\,(mm\,Hg)$ |
|---|---|---|---|---|---|
| 35 | 1.53 | 188.8 | 13.5 | 7.65 | 1.91 |
| $[10, 35]$ | 1.83 | 164.2 | 16.3 | 7.65 | 1.28 |
| 40 | 0.88 | 158.5 | 20.1 | 7.62 | 3.57 |
| $[10, 40]$ | 1.05 | 125.1 | 33.0 | 7.63 | 2.18 |
| 50 | – | – | – | – | – |
| $[10, 50]$ | 1.05 | 125.0 | 20.1 | 7.62 | 2.18 |

## REFERENCES


[1] Hayashi, T.T., (1977), Mechanics of Contact Lens Motion, *Ph.D Dissertation*, University of California.

[2] Moriarty, J.A., Terrill, E.L, (1996), Mathematical Modeling of the Motion of Hard Contact Lenses, *Euro. J. Appl. Math*, Vol 7, pp575-594.

[3] de Gennes, P-G., Quere, D., (2004), Capillary and Wetting Phenomena, Springer, New York.

[4] de Gennes, P-G., (1985), Wetting: Statics and Dynamics, *Reviews of Modern Physics*, Vol 57, pp827-863.

[5] Gao, L., McCarthy T.J., (2006), Contact Angle Hysteresis Explained, *American Chemical Society*, Vol 14, pp6234-6237.

[6] Joanny, J.F., de Gennes, P-G., (1984), A model for contact angle hysteresis, *American Institute of Physics*, Vol 81, pp552-562.

[7] Deen W.M., (1998), Analysis of Transport Phenomena, Oxford University Press, New York.

[8] Holt, V., (1997), Laser induced fluorescence measurement of the tear film thickness under a contact lens, *MSc Thesis*, Massachusetts Institute of Technology.

[9] Butt, H.J., Graf, K., Kappl, M., (2006), Physics and Chemistry of Interfaces, John Wiley & Sons, Weinheim.

[10] Wang, J., Fonn, D., Simpson, T.L., Jones, L., (2003), Precorneal and pre- and postlens tear film thickness measured indirectly with optical coherence tomography, *Investigative Ophthalmology and Visual Science*, pp2524-2528.

[11] Finn R., (1999), Capillary Surface Interfaces, *Notices Amer. Math. Soc.*, Vol 46, pp770.

[12] Frankel, T., (2004), The Geometry of Physics: An Introduction, Cambridge University Press, New York.

[13] Schulz, E., Simon, F., (1984), Contact lens fitting for binocular micromovement recording, *Graefe's Archive for Clinical and Experimental Ophthalmology*, Vol 221, pp282-285.

[14] Wang J., Cox I., Reindel W.T., (2009), Upper and Lower Tear Menisci on Contact Lenses, *Investigative Ophthalmology and Visual Science*, Vol 50, pp1106-1111.

[15] Gelfand, I.M., Fomin, S.V., Silverman, R.A., (2000), Calculus of Variations, Dover Publications, New York.

[16] Lemp, M.A., Holly, F.J., Iwata, S., Dohlman, C.H., (1970), The precorneal tear film: I. factors in spreading and maintaining a continuous tear film over the corneal surface, *Archives of Ophthalmology*, Vol 86, pp89-94.

[17] Braun, R.J., Fitt, A.D., (2003), Modeling drainage of the precorneal tear film after a blink, *Math. Med. Bio.* Vol 20, pp1-28.

[18] Raad, P.E., Sabau, A.S., Dynamics of a Gas Permeable Contact Lens During Blinking, *Journal of Applied Mechanics*, Vol 63, 411-418.

[19] Carney, L.G., Mainstone, J.C., Carkeet, A., Quinn, T.G., Hill, R.H., (1997), Rigid lens dynamics: Lid effects, *Contact lens association of Ophthalmologists*, Vol 23, pp69-77.

[20] Shanker, R.M., Ahmed, I., Bourassa, P.A., (1995), An in vitro technique for measuring contact angles on the corneal surface and its application to evaluate corneal wetting properties of water soluble polymers, *International Journal of Pharmaceutics*, Vol 119, pp149-163.

[21] Murgatroyd, H., Bembridge, J., (2008), Intraocular pressure, *Continuing Education in Anaesthesia, Critical Care & Pain*, Vol 8, pp100-103.

[22] French, K., (2005), Contact lens material properties: Part 1 Wettability, *www.opticianonline.net*, Vol 230, pp20-28.

[23] Athukorallage, B., (August 2012), Mathematical Modeling of a Contact Lens and Tear Layer at Equilibrium, *MSc Thesis*, Texas Tech University.